Bidctional vesicle motility: From molecular motors to Markov processes

Ietswaart, J.H.R.

J.H.R. Ietswaart

Bidirectional vesicle motility
from molecular motors to Markov processes

Bachelor thesis, July 3^{rd} 2009

Supervisors:
Physics: prof.dr. M. Dogterom
Mathematics: dr. F. Redig
direct supervisor Physics: P.M. Shaklee

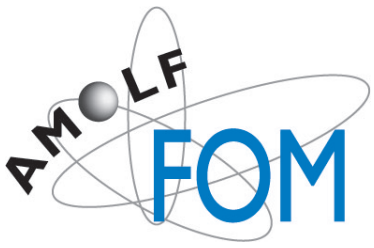

AMOLF
Mathematisch Instituut, Universiteit Leiden

Contents

Part I

1 Introduction

These first sections represent the physics part of the thesis. Vesicular transport inside a cell is known to be of importance for the movement of proteins from one compartment to another [1]. Small spherical transport vesicles are used as ferries for the proteins. We refer to these vesicles as small unilamellar vesicle (SUV) since their shell consists of one lipid bilayer.

In cells SUVs are directed along cytoskeletal filaments, the cellular railways. The SUV is the cargo and molecular motors are the engines that drive the cargo, attached to the motors, along the railway. In our case we focus on microtubules (MTs) as the railway. Microtubules are long biopolymer proteins with an intrinsic polarity. Tubulin dimers polymerize into protofilaments, that bundle then into a helical structure with 13 tubulin units in one turn, each coming from a different protofilaments. The N terminus is denoted by the plus end. Molecular motors are proteins that bind to a cytoskeletal filament and use the energy derived from repeated cycles of ATP hydrolysis to move steadily along it [1]. There are two types of microtubule motor proteins: kinesins and dyneins. Kinesin motors walk towards the plus end of an MT. Dyneins are a family of motors that move to the minus end. These two motors are essential for bidirectional transport *in vivo*.

One idea about how bidirectional vesicle transport is mediated, is informally called tug-of-war. In this scenario both type of motors are present and bound to the MT at the same time, so they feel each others pulling force mediated by the vesicle. Another idea is that the motors are turned on and off as a regulation [5]. Both experimentally and theoretically the tug-of-war model has been studied with kinesin en dynein motors rigidly coupled to beads in [7]. However *in vivo* the motors are allowed to diffuse through the membrane or selforganize in the vesicle.

In this study we imitate bidirectional vesicle transport *in vitro*. We prepare rhodamine labeled SUVs with a diameter of about 1 μm and attach both kinesin and dynein motors specifically to them. When the SUVs come into contact with MTs that are bound to a glass surface the SUVs are walked along the MT. We look at the position of the vesicle as it is transported. In this way we want to address the question: if bidirectional transport is force mediated, what behavior emerges? By differing the ratio of kinesins to dynein motors on the SUV, we want to see the influence of that on the motility of the vesicle. Furthermore we perform computer simulations with a developed model, a continuous time Markov chain based on principles from the model described in [3], to compare the idea of tug-of-war with the experimental results. Our findings are that SUVs driven by single kinesins move unidirectionally. SUVs driven by dyneins also move unidirectionally. SUVs covered with both type of motors move bidirectionally. As the ratio of kinesin to dynein goes up, the movement of the SUV becomes biased to one direction. When we compare these results to the situation *in vivo*, motor ratio could be a regulation mechanism, since at equal motor

Figure 1: First frame of a movie where an SUV (grey spot in the middle) covered with kinesin motors is transported along MT, indicated with the grey line. The SUV moves unidirectionally upwards.

concentrations the SUVs show not much movement, also seen in [15]. But at higher kinesin concentrations more movement in one direction is seen, which is necessary for axonal transport. The simulations suggest this as well, though the one directional distances traveled are longer than in the experiments.

2 Results

Figure 1 shows the first frame of a typical movie where an SUV is transported by motors. MTs decorating the surface below the SUV are not visible. Experiments were done for the following concentration proportions of kinesin concentration and dynein concentration (c_K, c_D): (100%,0%), (99%,1%), (95%,5%), (90%,10%), (75%,25%), (50%,50%), (0%,100%). After inspecting the direction of the movement by the SUV, we draw the grey line tracing the MT path below. To trace the position of the SUV in time we analyzed the intensity profile along the grey line. The resulting kymograph is shown in figure 2a. Here the vertical

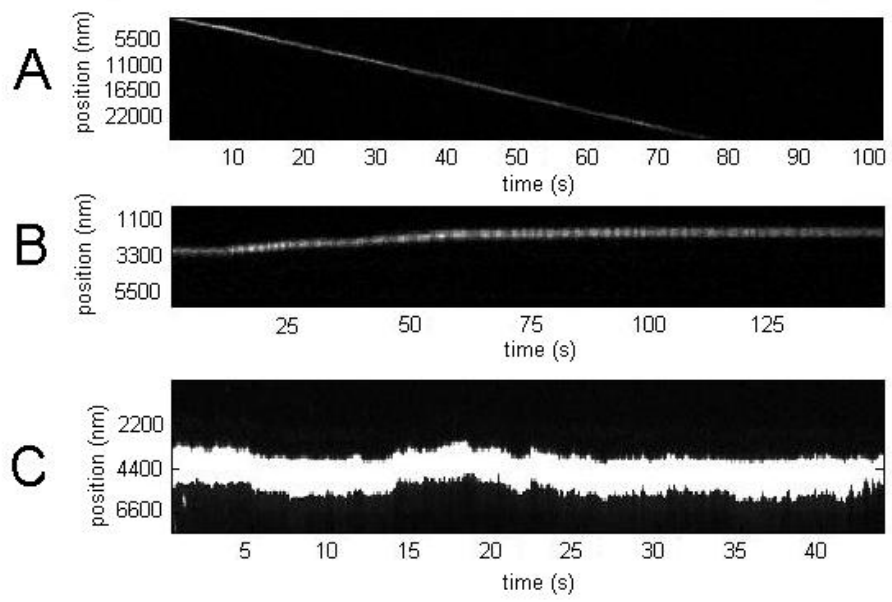

Figure 2: a: Kymograph of SUV from figure 1 covered with kinesin motors. The vertical axis is the grey line in figure 1 in nm and the horizontal axis denotes the time in s. The bright line is the path of the SUV along the grey line in time. b: Kymograph from a SUV covered with dynein motors. Image of SUV is not shown here. c: Kymograph from a SUV covered with (c_K, c_D)=(90%,10%) motors.

axis is the grey line from figure 1, the horizontal axis denotes the time. The bright line is a cross-section of the SUV moving in time. Figure 2b and 2c are kymographs of SUVs covered with respectively dynein only (2b) and concentration proportions (90%,10%) (2c). We have been precise with drawing the lines along which the kymographs are made, since changing the line a bit results in a different kymograph. The size of the effect can be significant when the SUV rotates as it is not always spherical.

To determine the precise location of the edge of the vesicle as it is displaced in time we set a threshold value as twice the background intensity. We determine the location at which the intensity exceeds the threshold value. After linear interpolation we determine the location of the edge of the SUV with subpixel resolution. This results in a position trace of the vesicle. The method gives accurate position trace for the kymographs in figure 2a and 2b (not shown here).In figure 3a we see the position for the SUV from kymograph 2c. We have thought of other ways to analyze the videos. But they all have their own difficulties. For instance particle tracking software is a nice way to determine the position in time properly, but then you obtain a 2D path instead of 1D, which gives rise to the question what can be considered as bidirected motion. Furthermore fluctuations in vesicle shape also bias the calculation of the position by particle tracking.

Others have shown that one dimensional diffusion along an MT can occur with dynein coated beads [17]. This implies that an assumption that vesicle movement is induced purely by the motors walking incorrect. For this we need to look at the speed distribution, since diffusion results in a much higher velocity than the single motor velocity for kinesin or dynein. The question arises how to analyze the velocity. We have chosen to calculate the instantaneous speeds. The instantaneous velocities are calculated as follows: for every t, we calculate position(t+windowsize)-position(t) and divide that by the window size to get the instantaneous velocity. The lower graph are instantaneous velocities calculated from this position with 4 different time window sizes (3b: 1s, 3c: 2s, 3d: 5s and 3e: 10s). As can be seen by comparing figure 4a and 4b the window size influences the speed distributions significantly. Still the fact that non zero velocities occur is clear.

For the traces of figure 2b and 2c, where only kinesin and only dynein are present, the method gives a peak around the value of the slope of the bright line in the kymographs (350 nm/s and 20 nm/s). We have tried to optimize the procedure such that non zero velocity peaks in the histograms are visible. Therefore most results are shown with a window size of 2s (= 20 data points) or 5s. When we apply the method to the simulations the single motor velocity peak of kinesin does appear, so this suggests that the analysis method can say something about the velocity with which the SUV moves. Velocities lower than 400 nm/s are measured. This suggests that the dynein motors do act as an opposing force. Figure 4 show histograms of the slope of figure 3c and 3d with window size 2 s and 5 s respectively. The red line indicates a gaussian fit of the histograms. We will use the mean μ and standard deviation σ to compare the results with the simulations and experiments without addition of ATP.

In figure 5 we compare the position traces of three SUVs all with a concentration ratio of (50%, 50%). Figure 5a has ATP, 5b does not and figure 5c is a position trace obtained by simulations. We notice that the simulation SUV moves 4 times farther than the real vesicle. According to [15] vesicle motile-activity is relatively low. In our experiments this is also the case. When we compare the SUV with ATP (figure 5b) to the case without ATP (figure 5c) we notice that the first has a maximum displacement of about 1μm, while the SUV without ATP displaces only 0.2 μm. This indicates the bidirected movement of the SUVs by motors, but the motility is not much higher (only 5 times) with walking motors. The displacement of 0.2μm could very well be noise due to our analysis method or thermal fluctuations while the SUV is bound to the MT.

For a better conclusion on the bidirected motion we refer to figure 6 that compares the velocity distributions calculated with window size 2s. belonging to respectively figure 5a, b and c. Figure 6a shows the experimental result with $(\mu, \sigma) = (8 \pm 2nm, 93 \pm 4nm)$, figure 6b everything is similar to figure 6a except that no ATP is added, so that the motors can not walk $(\mu, \sigma) = (3 \pm 2nm, 108 \pm 5nm)$. Finally 6c shows a histogram obtained by a simulation $(\mu, \sigma) = (17 \pm 1nm, 25 \pm 1nm)$. In the simulation a shoulder around 350 nm/s, the kinesin single motor velocity is visible in the histogram in contrast with the experiments. This indicates that there is a bias in the speed distribution in favor of the kinesin motors. The shoulder is not clearly visible in the real

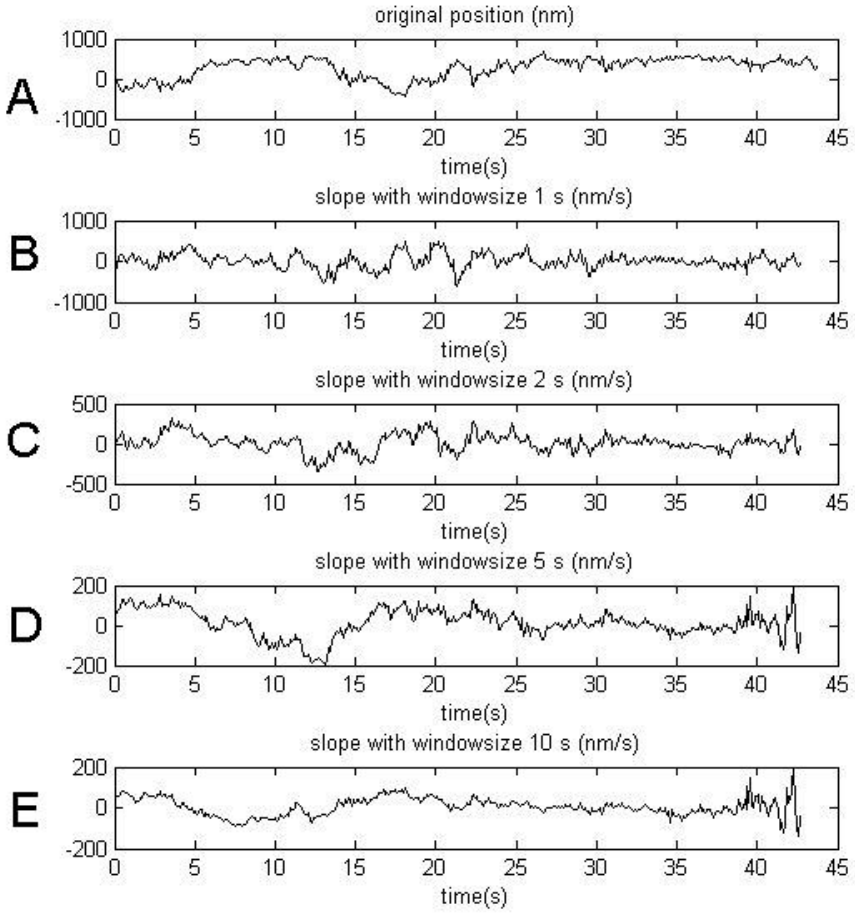

Figure 3: a: Position trace of the kymograph in figure 2c from a SUV with concentration ratio (90%,10%). The positions are there where the intensity in the kymograph exceeds the threshold value. , b: Instantaneous velocity as a function of time, calculated by position(t+window size)-position(t)/window size. Here the window size is 1s., c: Instantaneous velocity calculated with window size 2s., d: Instantaneous velocity calculated with window size 5s., e: instantaneous velocity calculated with window size 10s.

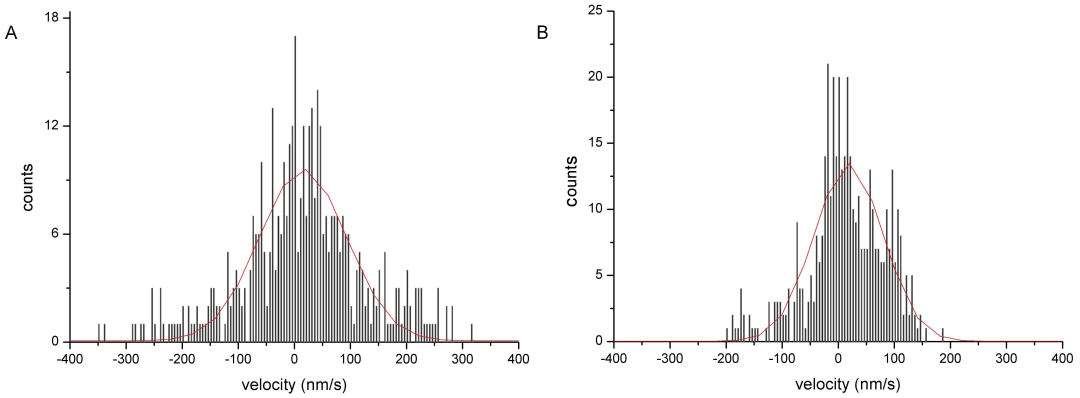

Figure 4: a: Histogram of instantaneous velocity calculated with a window size of 2s. The binsize for all histograms in this thesis is 5 nm/s. In red is the single gaussian fit of the histogram, b: Histogram of instantaneous velocity calculated with a window size of 5s. Again in red the single gaussian fit of the histogram. Notice that the width of the histogram is smaller in the 5 s. case. This is because for a larger window size the small fluctuations average out. Also the shape of the two histograms is different. in b there seems to be a little shoulder at 100 nm/s, which is not visible in a. This suggests that the window size influences the velocity distribution.

experiment with ATP, perhaps due to a low signal to noise ratio, though the velocity distribution is broader than the case where the motors can not walk. This is another indication for bidirected movement by motors. But the mean and spread of the gaussian fit of the simulation are lower than the than the experiment without ATP. This indicates that looking at the mean and spread of the fits is not always useful.

This becomes even more clear in figure 7 where the control and real experiments have similar mean and spread. So drawing conclusions only on the mean and standard deviation of the gaussian fits is the least trustworthy step in our analysis, since it does not distinguish between the experiments and simulations (see figure 7). Intuitively this is clear since fitting a single peak gaussian to the velocity histogram disguises the fact that possible other velocity peaks are present. We could look at the residuals, but then it is hard to say something quantitative about it again. Another argument is that figure 5a en 5b are not completely different, therefore it possible that there is in fact not more difference in the velocity distribution than we obtain via our analysis method. We have considered this thoroughly and present parameters of the gaussian fits in this thesis as the most systemic way to quantitatively summarize the measurements.

In figure 8 we see the scatter plots of all experiments without ATP. Since there is no walking possible the histograms should all result in a single peak around zero. The spread is a measure of how tightly the SUV is bound to the MT. We see that in general the controls of dynein have a lower spread than ki-

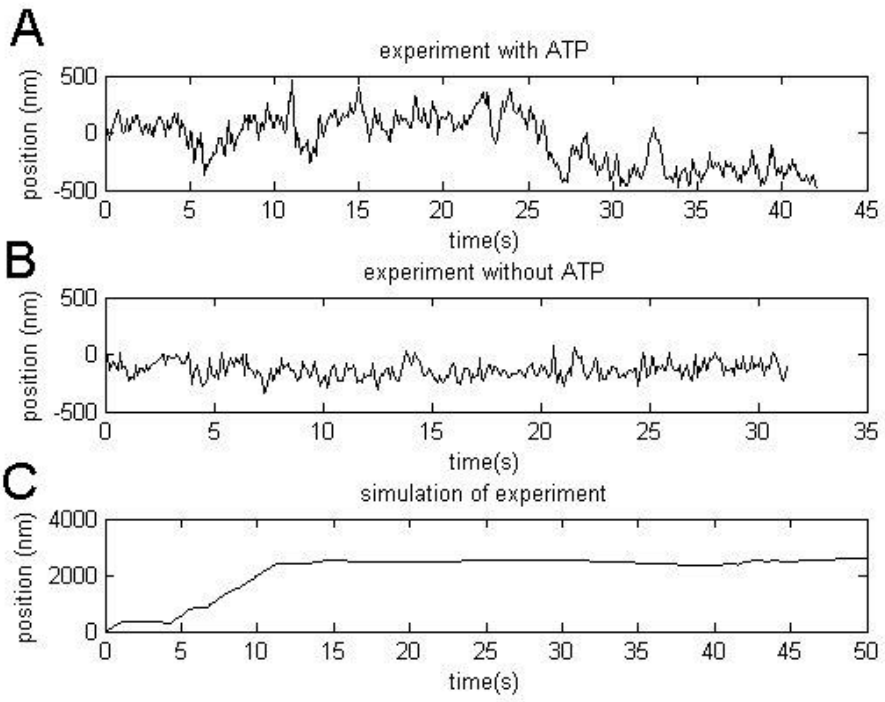

Figure 5: Three position traces calculated by setting a threshold value and for every time determining the location at which the intensity exceeds the threshold value. This value becomes the position. All three SUVs have a concentration ratio of (50%,50 %). a: Position trace from a real experiment, with ATP added so that the motors can walk. b: Also a real experiment, but no ATP was added, so no bidirected motion due to motors is possible. c: Position obtained by simulations (in all performed simulation the motors can walk). In the simulations the SUV moves farther compared to the real SUV, that moves more than the SUV without ATP.

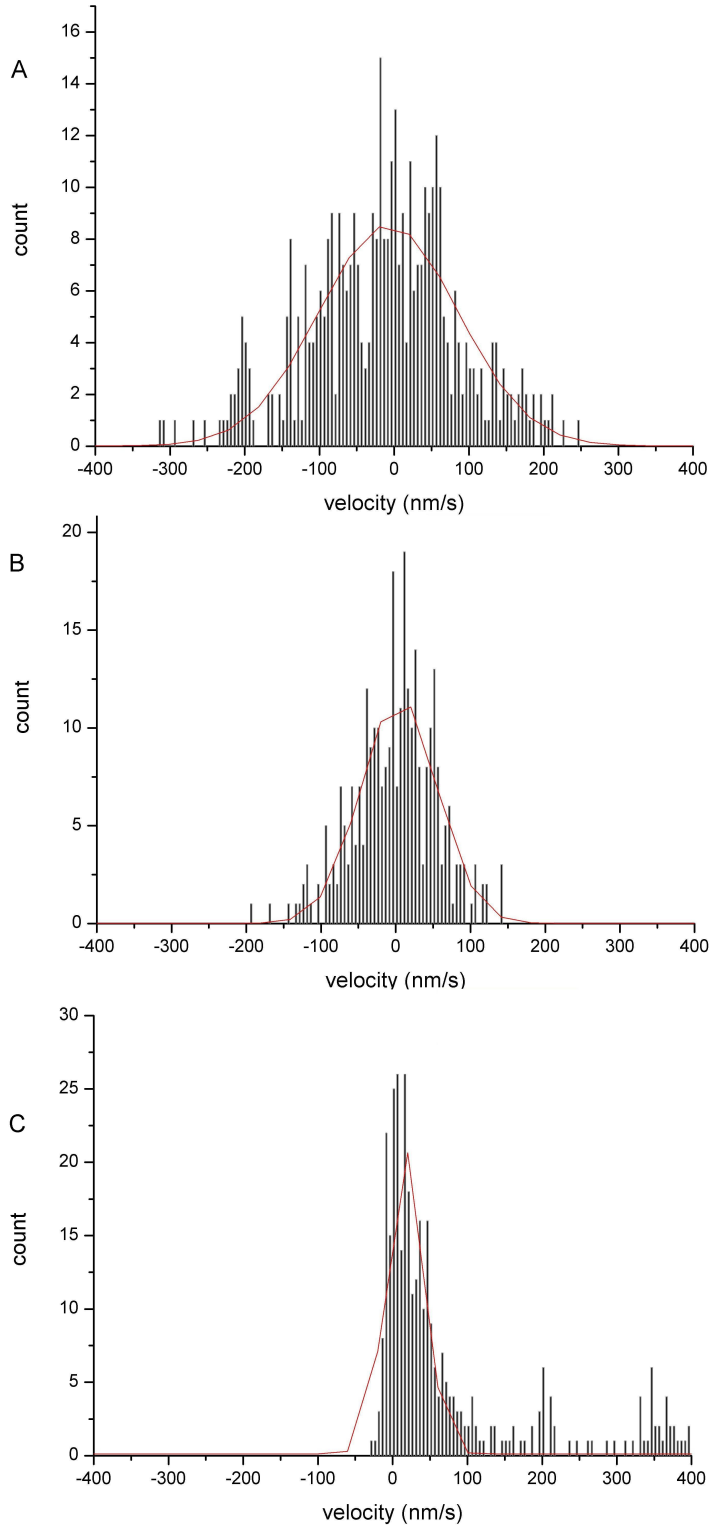

Figure 6: a: Histogram of instantaneous velocity calculated with a window size of 2s. from the trace of figure 5a. This is an SUV covered with motors with a ratio of (50%, 50%). ATP was added, so that the motors can walk. In red is the single gaussian fit of the histogram with parameters $(\mu, \sigma) = (8 \pm 2nm, 93 \pm 4nm)$, b:idem as a, but now from trace of figure 5b. No ATP was added, so the motors could not walk. In red the single gaussian fit of the histogram with parameters $(\mu, \sigma) = (3 \pm 2nm, 108 \pm 5nm)$, c:idem as b, but now from trace of figure 5c, the simulation. The single gaussian fit in red has parameters $(\mu, \sigma) = (17 \pm 1nm, 25 \pm 1nm)$, the histogram reveals a shoulder around 350 mn/s.

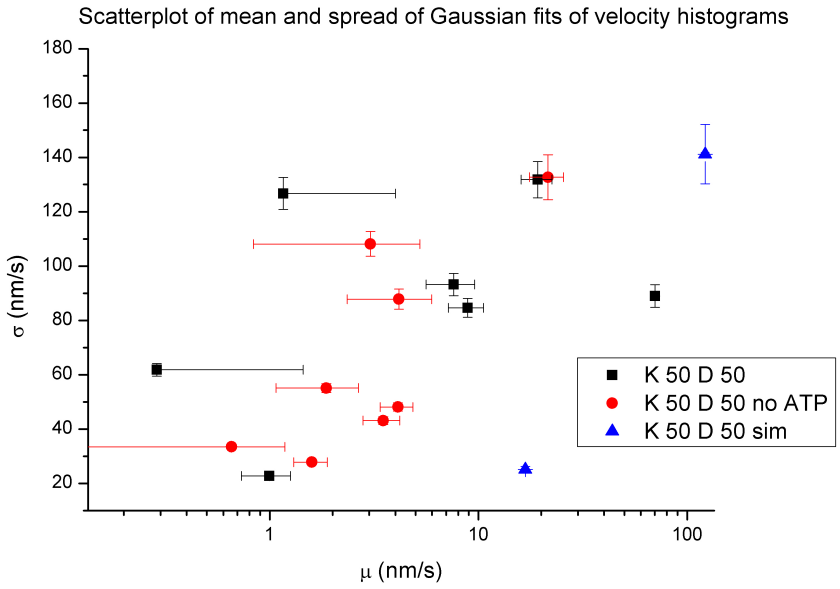

Figure 7: Scatter plot with the mean μ on a log scale and spread σ obtained by fitting a single gaussian to the histograms of the slopes with window size 2s. of SUVs with a concentration ratio (50%,50%). The error bars indicate the uncertainty of the fits. All data points have a mean lower than 10 nm/s and a spread lower than 150 nm/s. This means that by looking at mean and spread we can not distinguish between different experiments. The blue data point with the lowest spread represents the fit in figure 7c, where a clear shoulder at 350 nm/s can be seen. This suggests that the analysis method is not optimal in this case to determine velocities other than zero.

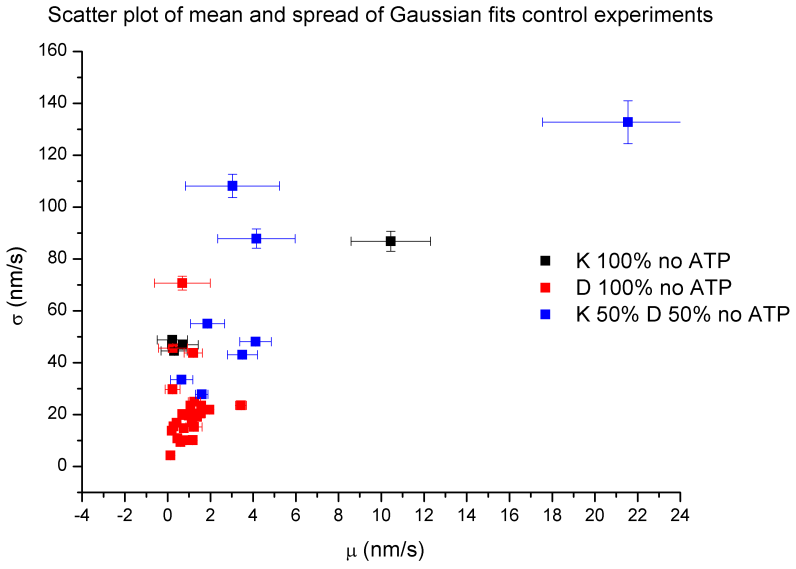

Figure 8: Scatter plot with the mean μ and spread σ obtained by fitting a single gaussian to the histograms of the slopes with window size 2s. of experiments where no ATP was added. This means that the motors can not walk. We see indeed that al means are below 25 nm/s. In general the dynein covered SUV have a lower spread in the velocity which indicates that it is more tightly bound the MT than SUVs covered with kinesin. SUVs with a concentration ratio of (50%, 50%) have even higher spread than kinesin which suggests that those SUVs are even more loosely bound to the MT.

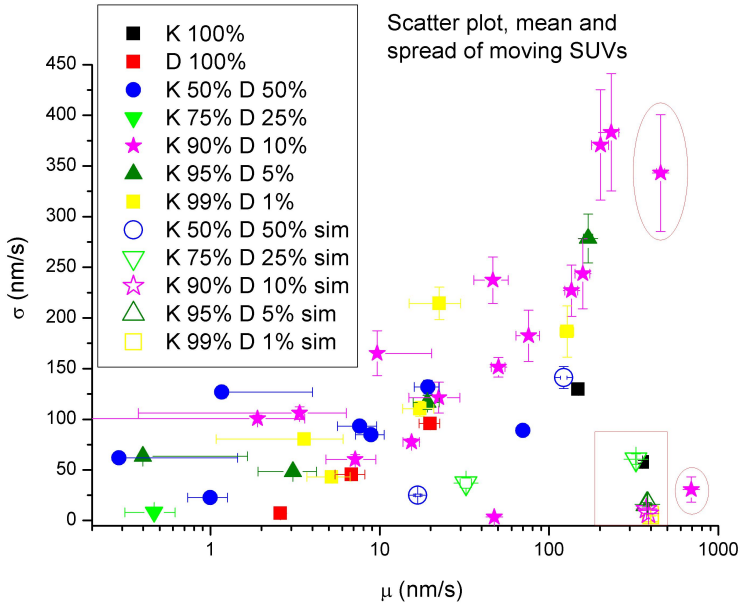

Figure 9: Scatter plot with the mean μ on a log scale and spread σ obtained by fitting a single gaussian to the histograms of the slopes with window size 2s. of moving SUVs. The error bars indicate the uncertainty of the fits. Simulations and real data with the same concentration ratios have the same symbols and border colors. The simulations have a white interior in contrast to the real data with filled colors. The red circles emphasize the two data points with a mean higher than the single motor velocity. Inside the red rectangle are data points with a mean close to the single motor speed of kinesin (400nm/s).

nesin and the mixture has the biggest spread. That suggests that dynein motors are more tightly bound to the MTs than kinesin motors. And a vesicle which has both dynein and kinesin motors attached to it is even more loosely bound.

We end the results part with a scatter plot of all moving SUVs shown in figure 9. Experiments with different ratios of kinesin to dynein motors are done to investigate the dependence of the motility of an SUV to the motor population. First we notice that two of the 90% K 10% D show a mean that is above the single motor velocity of kinesin (data points in the red circles. We suggest that this is due to diffusion [17]. Secondly there seems to be the trend that as the kinesin motor density goes up, both mean and spread go up. We suggest that as the ratio favors kinesin, the SUV becomes more motile, since in the single motor velocity of kinesin is higher. There are measurements from 90% K 10% D that have higher mean and spread than 95 and 99 % K. There are several possible explanations for this. The first one is that the motors do not bind homogeneously, but cooperatively in the sense that it is more likely that one type of motor can dominate so that the other type of motors get pulled off more frequently. In this way the motor ratio is not representative for the number of motors that are bound on the MT. Another explanation could be that

pipetting errors are responsible for other motor ratios in our experiments than we calculated. The reason that we did not try a motor ratio which favor dynein, is that the motility of the SUV is hard to identify because of the slow single motor speed (40nm/s) and the fact that an unknown fraction of the dynein motors is dead. This introduces experimental challenges that are difficult to account for.

Furthermore in the simulations there is really the trend that at higher kinesin density the mean shifts from around 0 to around the single motor velocity of 400 nm/s in the simulations. And experimental verification (100% K) agrees with that value. A possible explanation for this is that is depends on the specific SUV movement: when the SUV sits still for a long time the zero velocity peak dominates, but when SUV moves a considerable time due to the kinesin motors walking, the non zero peak becomes significant, so the mean shifts to a position in between the two contributions and the spread increases accordingly.

Finally we discuss some remarks on our simulations. We see repetitively that in the simulations the SUV moves a larger distance than in our experiments (see for example figure 5). Some suggestions to improve our model are: use a three lane model instead of a one lane, since an MT has multiple parallel binding sites [3]. If we combine that with the rule in our code that if a dynein motor is situated at site 1 the SUV can not move since the kinesin motors are not strong enough to pull the dynein motor off, then perhaps the SUV becomes less motile. Furthermore we have approximated dynein's dead motor fraction by reducing the motility of all single dynein motors and the unbinding probability. But is would be better to really introduce three sorts of motors: walking dyneins, dead dyneins and kinesins. Another possible improvement would be to make the single motor velocity force dependent [2] Because of lack of time I did not get to these implementations.

3 Conclusion and discussion

We have examined SUV transport along MTs driven by molecular motors of two types, kinesin and dynein. We varied the concentration ratios (c_K, c_D) to see if this influences the motility of the SUVs. Our findings are that SUVs driven by single kinesins move unidirectionally. SUVs driven by dyneins also move unidirectionally, though a fraction of dead motors negatively influences the motility. SUVs covered with both type of motors move bidirectionally. As the ratio of kinesin to dynein goes up, the movement of the SUV becomes biased to one direction. When we compare these results to the situation *in vivo*, motor ratio could be a regulation mechanism, since at equal motor concentrations the SUVs do not show much movement, also seen in [15]. But at higher kinesin concentrations more movement in one direction is seen, which is necessary for axonal transport. The simulations suggest this as well, though the net distances traveled are longer than in the real experiments. Further adjustments on the microscopic details are needed to improve the model for the simulations. From the experiments without ATP we confirm that dynein motors are more tightly bound to the MTs than kinesin motors. When the SUVs are covered with both dynein en kinesin without the addition of ATP, they are the least tightly bound to the MT. Further experiments with dynein motors that walk faster

could reveal more of the motility of the SUVs. Tipping the concentration ratio towards dynein is then a logical continuation. Also a smaller fraction of dead motors is likely to influence the behavior. A last suggestion is use dynein motors that are known to be completely immobile.

4 Methods and materials

4.1 Experiments

All lipids are purchased from Avanti Polar Lipids. The lipid mixture consists of 94.9 mol% 1,2-di-(9Z-octadecenoyl)-sn-glycero-3-phosphocholine(DOPC), 4 mol% 1,2-dioleoyl-sn-glycero-3-phosphoethanolamine-N-[methoxy(polyethylene glycol)-2000] (PEG(2000)-DOPE), 1 mol% 1,2-distearoyl-sn-glycero-3-phospho ethanolamine-N-[biotinyl(polyethylene glycol)-2000](Bio-PEG(2000)-DSPE), 0.1 mol% 2-dioleoyl-sn-glycero-3-phosphoethanolamine-N-(lissamine rhodamine B sulfonyl)(TRITC-DOPE). The small unilamellar vesicles were preparated by a method called the freeze-thaw-sonication method [13]. First the lipids are suspended in chloroform and mixed together (total weight 0.5 mg) after which the mixture is dried with nitrogen. Then it is suspended in 50 mM (600 μl) KCl and 5 times subsequently frozen and thawed. Finally the vesicles are sonicated for 15 min. If the mixture is still milky, SUVs are not fully formed and the freeze-thaw-sonication cycle is repeated. At last the SUVs were checked under the microscope.

The microtubules were polymerized by the following standard procedure. 2 μl tubulin, 0.4 μl GTP (50mM) and 2.5 μl MRB80 (80 mM K-Pipes/1 mM EGTA/4 mM MgCl2) were mixed on ice and incubated at 37°C for 13 min. Afterwards the MTs were stabilized with 70 μl of 10 μM taxol in MRB80 (taxol buffer).

Coverslips were cleaned and preparated with N-[3-(trimethoxysilyl)-propyl] demethylenetriamine (DETA) as described in [16]. A coverslide was wiped clean with ethanol and the flow chamber was put together consisting of the coverslip put on top of two lanes of vacuum grease on the coverslide. All incubations were at room temperature. 1.5 μl of MTs diluted with 13.5 μl of taxol buffer were flowed into the chamber and incubated for 10 min. Then the chamber was rinsed twice with taxol buffer. 0.4 mg/ml casein in taxol buffer was incubated in the chamber for 7 minutes. Finally the chamber was rinsed two more times with taxol buffer. In parallel 1 μl Streptavidin (2 mg/ml) was added to 13 μl of 1:500 diluted SUV mix and incubated for 10 min. Then 1 μl of motors (kinesin and/or dynein) was added and incubated for 10 min. The motors were purified as described in [18](kinesin) and [11](dynein). Finally glucose (0.2μl), oxygen scavenger (0.2μl), ATP (0.3μl of 100mM MgATP), methylcellulose (0.5μl) and taxol/casein buffer (0.5μl of 0.4mg/ml) were added to the SUV mix.

Data was acquired on a spinning disc microscope comprised of a confocal scanner unit (CSU22, Yokogawa Electric Corp.) attached to an inverted microscope (DMIRB, Leica) equipped with a 100x/1.3 NA oil immersion lens (PL FLUOTAR, Leica) and a built-in 1.5x magnification changer lens. The sample was

illuminated using a 514 nm laser (Coherent Inc.). Images were captured by an EM-CCD (C9100, Hamamatsu Photonics) controlled by software from VisiTech International. Images were acquired with a 100ms exposure at 10Hz. The data were stacked .tiff square images of 512 pixels. Kymographs were made in imageJ and further analysed with MATLAB and Origin.

4.2 Model of SUVs and simulations

The introduction explained several possible mechanisms for bidirectional transport along microtubules. We assume the transport is not regulated by any cofactors and that the motors are the only proteins that influence the motility of the SUV. In order to make quantitative predictions on the movement of the SUVs we introduce a model system. We discretize the SUV into parts of $a = 8$ nm, the lattice spacing of a microtubule [3]. In figure 10, a cartoon modified

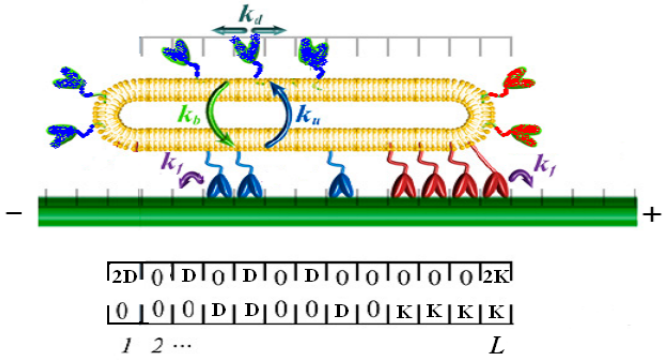

Figure 10: Cartoon of an SUV with kinesin (shown in red)and dynein (shown in blue) motors bound to it. The MT lattice is shown near the green thick line that represents the MT. The membrane lattice is shown above the vesicle. Underneath the MT we see the resulting configuration. K represents a kinesin motor and D a dynein. The sites are numbered 1 up to L. Different parameters are used, the rate to step forward (different values for K and D), the binding rate, the unbinding rate, and the diffusion rate.

from Campàs [3], we illustrate the model system. We divide the SUV into two discrete lattices, one on the MT and another that we call the membrane lattice. We ignore the three dimensional shape of the SUV because we approximate the MT as a one dimensional structure and we assume that only one motor can attach to a binding place on the MT (along a single protofilament) [1], so that the position of the motors only fall in one dimension. We are interested in the position of the single motors along the membrane and MT lattice. The membrane lattice corresponds to the part of the SUV that is not near the MT. Here the motors freely diffuse because they are not bound to a MT and they can therefore occupy the same site. And as noted above, a motor that is on the MT lattice is assumed to be bound to the MT. In this way only one motor can be at a site of the MT lattice. Figure 11 gives an example of a possible configuration for a SUV that is of diameter $L \cdot a$, where L is the number of consecutive sites. The lower grid denotes the MT lattice and the upper one the membrane lattice. K denotes a kinesin motor and D a dynein.

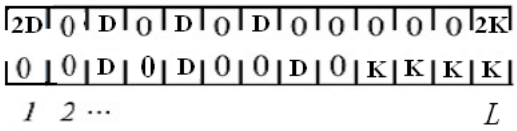

Figure 11: An example of a configuration. The lower grid represents the MT lattice, the upper one the membrane layer. Every box is referred to as a site, which can be empty, a kinesin (K) can be bound at that site or a dynein motor (D) can be bound. In the membrane layer multiple motors can occupy one site, as we see at site 1 and site L.

We determine S, the space of all possible configurations. We fix a number of kinesin motors, N_K, and for dynein, N_D. Then S can be constructed as follows.

$$S_{MT} := \{f | f : \{1, 2....L\} \to \{0, D, K\}\}$$

$$S_M := \{g | g : \{1, 2....L\} \to \{0, K, ..., N_K \cdot K\} \times \{0, D, ..., N_D \cdot D\}\}$$

$$S := \left\{ (f, g) | f \in S_{MT}, g \in S_M, \sum_{i=1}^{L} f(i) + g(i) = N_K \cdot K + N_D \cdot D \right\}$$

Where S_{MT} is the space of configurations of the MT lattice and S_M the state space of the membrane lattice. We will denote throughout this thesis an element of S by η and ignore in this notation the fact that it is a function because it is rarely needed, except in the definition of the position of the SUV. For that we define $\eta_i = f(i)$ and $\eta^i = g(i)$ if $\eta = (f, g) \in S$ with $i \in \{1, 2....L\}$. So, for instance $\eta_L = K$ if the configuration is of the form as shown in 12. Whenever a

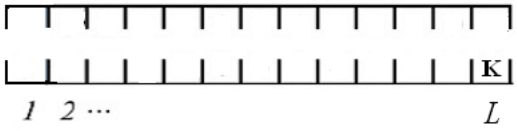

Figure 12: A configuration of a SUV with diameter $L \cdot a$ with unspecified site occupation except for site L of the MT lattice, which is occupied with a kinesin motor. This is denoted by $\eta_L = K$.

certain motor steps, binds or unbinds to/from the MT or diffuses the configuration changes. We call this a jump or transition from configuration η to η', both elements of S. The times at which the jump $\eta \mapsto \eta'$ occur, follow a Poissonian distribution with a rate $q(\eta, \eta')$. We use the hardcore exclusion principle for the MT lattice and individual motors can step forward, bind from the membrane lattice to the MT lattice, unbind from the MT to the membrane or diffuse in the membrane layer. For more details on the possible transitions I refer to appendix A. The associated single motor rates $(k_f^K, k_f^D, k_b, k_u, k_d)$ are all known parameters, obtained either via the literature or by measurement. Table 1 gives the single motor rates, also indicated in figure 10.

parameter	value	source
k_f^K	$50s^{-1}$	single motor velocity V^K measured, and $k_f^K = \frac{V^K}{a}$
k_f^D	$5s^{-1}$	single motor velocity V^D measured, and $k_f^D = \frac{V^D}{a}$
k_b	$4.7s^{-1}$	[3]
k_u	$0.42s^{-1}$	[3]
k_d	$0.42s^{-1}$	[3] measured diffusion constant D, and $k_d = \frac{D}{a^2}$

Table 1: Numerical values of the single motor parameters that are used in the model. The source indicates whether the values are obtained by measurement ourselves (measured) or by others (article reference)

Finally we want specify what movement of an SUV means in the context of our model. Motors at he ends of the SUVs (sites 1 and L) that are bound to the MT are the only motors that feel load. These motors are influenced by motors on the other side of the SUV that want to step in the opposite direction. Motors in the rest of the SUV (all sites except for 1 and L) walk through a fluid bilayer and therefore do not feel any load. As kinesin walks towards the plus end of the MT, the SUV makes a step of 8 nm when a transition occurs in which $\eta_L = K$ and specifically that K takes a step. An example of such an transition is given in figure 13. Notice that the lattice (which represents the SUV) shifts along with the kinesin at the end. The motors that are bound to the MT do not shift along. Now we define the set R^+ that contains transitions $\eta \mapsto \eta'$ in which the

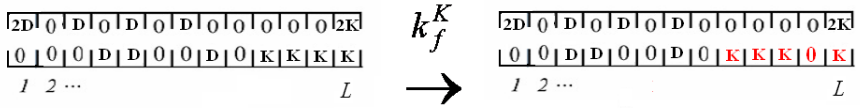

Figure 13: Transition from the left configuration to the right in which the kinesin motor bound to the MT at site L makes a step forward. The lattice shifts along but the bound motors stay put. The position function Z_t increases with 8 nm as this jumps occurs.

kinesin motor $\eta_L = K$ steps forward, i.e. the transitions in which a lattice shift occurs. Analogously R^- is formed by the transitions $\eta \mapsto \eta'$ with $\eta_1 = D$ steps forward (towards the minus end of the MT). Thus we define position Z_t of the SUV as

$$Z_t = a \cdot \sum_{\eta \mapsto \eta' \in R^+} |\{\eta \mapsto \eta' at\ s, s \in [0,t]\}| - a \cdot \sum_{\widetilde{\eta} \mapsto \widetilde{\eta}' \in R^-} |\{\widetilde{\eta} \mapsto \widetilde{\eta}' at\ \widetilde{s}, \widetilde{s} \in [0,t]\}|$$

This expression simply tells how many transitions from R^+ occurred in the time interval $[0,t]$ and multiplies this with the lattice spacing a (=8 nm) which is equal to the distance that kinesin motor pulls towards the plus end. Then of course we must subtract the displacement in the minus direction.

In appendix A we find two matlab codes for the simulations. The codes were

adapted from an existing code in the group one used to simulate motor dynamics in a similar manner. There we specify the transitions that are element of R^+ and R^-. Because the model is a Markov chain, this process can be simulated with a Gillespie algorithm [3], but the structure of the codes is a little different since we do not have Poissonian times at which the configuration changes, but after a fixed time interval the motors do something with a probability that is derived from the rates of the jumps. In this way we approximate the Gillespie algorithm. For details on and differences between the codes we refer to appendix A. In section 3 all simulations were performed with the code tugowar-deadmotors.

Part II

5 Construction of continuous time Markov chains

The following sections are the mathematics part of this thesis. The aim is to investigate the formal mathematical structures behind the model introduced in section 4.2 and derive theorems for these structures. As we know from section 4.2 we want to model the motility of SUVs under the influence of kinesin en dynein motors. Therefore we construct a stochastic process which includes the following idea: once you know the position of every motor, it does not matter for the future behavior of the SUV, how the motors got there. This is plausible because at any time motors have a constant rate with which they bind, unbind or walk. This idea is an instance of the Markov property. We'll make that more precise by defining the Markov process, a process with exactly that property [14].

We begin with some definitions that are taken from [12]. A probability measure is a triplet $(\Omega, \mathcal{F}, \mathbf{P})$ with Ω a set on which a σ-algebra $\mathcal{F}$ is defined. $\mathbf{P}$ is a probability measure, i.e. a measure on $\mathcal{F}$ with the restriction that $\mathbf{P}(\Omega) = 1$. From now on we assume that when we speak of a measure, it is in fact a probability measure. $E \in \mathcal{F}$ is called an event. Now let $(S, \mathcal{A})$ be a measurable space. We refer to S as the state space, or configuration space. A random variable X from Ω to S is a $(\mathcal{F}/\mathcal{A})$-measurable map $X : \Omega \to S$. Almost surely is just a saying for almost everywhere with respect to a probability measure. Finally X is a stochastic process when $X = \{X_t : 0 \leq t < \infty\}$ holds with $\forall t : X_t$ a $(S, \mathcal{A})$-valued random variable from $(\Omega, \mathcal{F}, \mathbf{P})$.

After these general definitions from probability theory we proceed with defining the Markov process, a special kind of stochastic process. let Y be a metric space with the Borel σ-algebra, analogous to $(S, \mathcal{G})$ and likewise let Ω be equal to D_Y, the space of right continuous functions with left limits (RCLL functions) from $[0, \infty)$ into Y. So the followings holds for $\omega \in D_Y$: $\forall t \in [0, \infty) : \omega(t) = \lim_{s \downarrow t} \omega(s)$ and the limit $\omega(t^-) = \lim_{s \uparrow t} \omega(s)$ exists. Think of it as ω being a path in Y. Our process $X = \{X_t : t \geq 0\}$ now consists of the coordinate mappings $X_t : D_Y \to Y$ with $X_t(\omega) = \omega(t)$, which tells us the configuration the system is in at time t. Now for our purposes we confine ourselves to Y being countable, then the singletons η with $\eta \in Y$ are measurable. If we want X to become a stochastic process we need every X_t to be measurable. We construct now $\mathcal{F}$ in such a way that we have this desired property.

We define $\mathcal{E}$ as the set of subsets E of D_Y that are of the form:

$$E = X_t^{-1}(\eta) = \{\omega \in D_Y : \omega(t) = \eta\}$$

Then we define $\mathcal{F} := \sigma(\mathcal{E})$, the σ-algebra generated by $\mathcal{E}$. A shorthand notation for this is: $\mathcal{F} =: \sigma\{X_t : t \geq 0\}$ and similarly $\mathcal{F}_t := \sigma\{X_s : t \geq s \geq 0\}$. We will use this notation later on. Notice that now X_t is $\mathcal{F}$-measurable for every $t \geq 0$.

Let $\theta_t : D_Y \to D_Y$ be the shift map defined by $\theta_t\omega(s) = \omega(t+s)$. $\theta_t\omega$ is the path that starts at $\omega(t)$ and walks along ω onwards. For an event $A \in \mathcal{F}$: $\theta_t^{-1}A = \{\omega : \theta_t\omega \in A\}$ and it can be seen as the event that A happens from time t onwards. After all these preparations we are now ready for the definition of a (countable state) Markov process[14]. As we have chosen Y to be countable this process is also referred to as a continuous time Markov chain.

Definition 1. *A Markov process is a collection $\{P^\eta : \eta \in Y\}$ of probability measures on D_Y with these properties:*

1. $P^\eta\{\omega \in D_Y : \omega(0) = \eta\} = 1$
2. $P^\eta[\theta_t^{-1}A|\mathcal{F}_t](\omega) = P^{\omega(t)}(A)$ *for P^η-almost every ω, for every $\eta \in Y$ and $A \in \mathcal{F}$*

The first requirement states that η is the configuration in which the process starts under the measure P^η. Notice that is does make sense to have a measure P^η for every starting point because not every path will be equally probable when the begin state is changed. The second requirement is exactly the Markov property. The object on the left hand side is the probability that concerns the future from time t onwards given that we know the past up to time t. In a Markov process this is equal to the probability to start in $\omega(t)$. A thorough reader might object that we haven't defined conditional probability yet. This is of course true. In fact $P^\eta[A|\mathcal{F}_t](\omega) = \mathbb{E}^\eta(\mathbf{1}_A|\mathcal{F}_t) \cdot \mathbf{1}_A$, with $\mathbf{1}_A$ the indicator of A. For the definition of $\mathbb{E}^\eta(\mathbf{1}_A|\mathcal{F}_t)$, a conditional expectation, we refer to appendix C on martingale theory. The (unconditional) expectation $\mathbb{E}^\eta[g]$ of a measurable function $g : D_Y \to \mathbb{R}$ is defined by:

$$\mathbb{E}^\eta[g] = \int g(\omega)P^\eta(d\omega)$$

6 Generators and properties of Markov processes

After this rather abstract section, let us focus on our objectives once more. We want to model the motility of SUVs but all we know are the different states the model can be in and the rates at which they jump from one configuration to another. These rates are in fact important for Markov chains. Since we have a countable state space we can ask ourselves: starting from state η what is the probability to be in η' at time t. Let us call this probability $p_t(\eta, \eta')$, then we have the following equality:

$$p_t(\eta, \eta') = P^\eta[\{\omega : \omega(t) = \eta'\}]$$

This probability returns in a linear operator on $C_b(Y)$ called the generator L. Let X be a Markov process as described above. Furthermore $C_b(Y)$ is the

space of bounded functionals endowed with the supremum norm, which makes it a Banach space. This makes sure that the image $\mathrm{L}f$ exists and that is has nice continuity properties.

Definition 2. *The operator* $\mathrm{L} : C_b(Y) \to C_b(Y)$ *is called the generator of* X *if*

$$\mathrm{L}f(\eta) = \lim_{t \to 0} \frac{\mathbb{E}^\eta[f(\omega(t)] - f(\eta)}{t}$$

In a countable state space the domain is indeed $C_b(Y)$ completely, but in general the limit does not exist for every $f \in C_b(Y)$. But we focus on a countable space. In that case the generator reduces even further to:

$$\mathrm{L}f(\eta) = \sum_{\eta' \in Y} q(\eta, \eta')[f(\eta') - f(\eta)]$$

with $q(\eta, \eta') = \frac{d}{dt} p_t(\eta, \eta')$ We see that the derivative of the probability to go from η to η' appears. It is called a rate. They can be seen as the average velocity at which a jump from η tot η' occurs [14]. This is exactly what we know in our model. So we have now an expression for the generator. It appears to be important for several quantities that we are interested in. For instance the average velocity of the SUV. To get there we need a notion of invariance or equilibrium. After that we discuss a theorem which relates the generator and an invariant measure. Then we will be able to calculate the average velocity of the SUV.

A measure μ on Y is an invariant measure for a Markov process if $\forall f \in C_b(Y)$ and $\forall t \geq 0$:

$$\int \mathbb{E}^\eta[f(\omega(t)]\mu(d\eta) = \int f(\eta)\mu(d\eta)$$

To make this definition more clear, we look at the left hand side fist. Although $f \in C_b(Y)$, not in $C_b(D_Y)$ we can see it as though it sends ω to $f(\omega(t)$. So the expectation is well defined. Notice that when t is held fixed, $\mathbb{E}^\eta[f(\omega(t)]$ is a (bounded) function from Y into $\mathbb{R}$, so it is an element of $C_b(Y)$. But when η is fixed, it is a function from $[0, \infty)$. Because Y is countable $\eta \mapsto \mathbb{E}^\eta[f(\omega(t)]$ is measurable. We use both properties in this definition because for invariance we expect the left hand side to be independent of time and integrated over the state space, the expectation of f should be equal to f. Invariance means that the probability to be in state η is constant over time [14]. Like most physical systems, our Markov process will converge to such an equilibrium.

As noted earlier $\mathrm{L}f$ is the expected infinitesimal change of f. We can now elegantly link this to invariance [14]:

Theorem 1. *Let* μ *be a probability measure on* Y *and and* L *the generator of* X*, then* μ *is invariant for* X *if and only if* $\forall f \in C_b(Y)$*:*

$$\int \mathrm{L}f d\mu = 0$$

Proof. $\Rightarrow$ Let $f \in C_b(Y)$ and μ invariant for X, then because convergence in the supremum norm is uniform convergence we have

$$\int \mathrm{L}f d\mu = \int \lim_{t \to 0} \frac{\mathbb{E}^\eta[f(\omega(t)] - f(\eta)}{t} d\mu$$

$$= \lim_{t \to 0} \frac{1}{t} \left[\int \mathbb{E}^\eta [f(\omega(t))] d\mu - \int f(\eta) d\mu \right] = 0$$

The last step comes of course from the invariance of μ
$\Leftarrow$ Assume that for all $g \in C_b(Y)$ $\int \mathrm{L} g d\mu = 0$, choose now a $f \in C_b(Y)$, then we know from lemma 1 that

$$\frac{d}{dt} \mathbb{E}^\eta \left[f(\omega(t)) \right] = L \left[\mathbb{E}^\eta \left[f(\omega(t)) \right] \right]$$

Integrating both sides gives us

$$\int_0^t \mathrm{L} \left[\mathbb{E}^\eta \left[f(\omega(s)) \right] \right] ds = \int_0^t \frac{d}{ds} \mathbb{E}^\eta [f(\omega(s))] ds$$

$$= \mathbb{E}^\eta [f(\omega(t)] - \mathbb{E}^\eta [f(\omega(0))]$$

But $\omega(0)$ is by assumption η so the second term is just f evaluated in η. Now we integrate over the state space with respect to μ and use Fubini's theorem:

$$\int_0^t \left(\int \mathrm{L} \left[\mathbb{E}^\eta \left[f(\omega(s)) \right] \right] d\mu \right) ds = \int \mathbb{E}^\eta [f(\omega(t)] d\mu - \int f(\eta) d\mu$$

We saw that for fixed t, $\mathbb{E}^\eta [f(\omega(t)]$ lies in $C_b(Y)$, so the state space integral is 0 for all t. This gives us the desired result: for all $t \geq 0$

$$0 = \int \mathbb{E}^\eta [f(\omega(t)] d\mu - \int f(\eta) d\mu$$

□

In the section with applications we will see that we need μ for the calculation of the average speed of the SUV. To find μ, we use theorem 1. In our model the state space is finite, so we can see L as a matrix: $\mathrm{L} = (q(\eta, \eta'))_{\eta, \eta' \in S}$ and $f(\eta)$ as a column vector and $\mu(\eta)$ as a row vector. So requiring that the right hand side of the theorem is true, is in fact equivalent to saying that $\mu \mathrm{L} = 0$, with 0 the row vector filled with zeros. This is a finite system of linear equations that we can solve with techniques from linear algebra. Existence and uniqueness issues for μ are then immediately resolved.

The last important property of Markov processes that we need, is the following theorem [14]. For details about martingale theory we refer to appendix C.

Theorem 2. *Let X be a Markov process with generator* L *then for any $f \in C_b(Y)$ the process M with*

$$M_t = f(X_t) - f(X_0) - \int_0^t \mathrm{L} f(X_s) ds \tag{1}$$

is a martingale with respect to the filtration $\{\mathcal{F}_t\}_{t \geq 0}$

Proof. M is adapted by construction of every $\mathcal{F}_t$. Secondly fix a $t \geq 0$ then

$$\mathbb{E}^{X_0}\left[|M_t|\right] \leq 2\|f\|_\infty + t\|\mathrm{L}f\|_\infty < \infty$$

because both f and $\mathrm{L}f$ are bounded. For the last requirement fix an $s \geq 0$, we start with the first two terms:

$$\mathbb{E}^{X_0}\left[f(X_t) - f(X_0)|\mathcal{F}_s\right] = \mathbb{E}^{X_s}\left[f(X_{t-s})\right] - f(X_0)$$

by the use of Markov property 2. from definition 1. The second terms comes out because of (7). We proceed with the integral term, by (8):

$$\mathbb{E}^{X_0}\left[\int_0^t \mathrm{L}f(X_r)dr|\mathcal{F}_s\right] = \mathbb{E}^{X_0}\left[\int_0^s \mathrm{L}f(X_r)dr|\mathcal{F}_s\right] + \mathbb{E}^{X_0}\left[\int_s^t \mathrm{L}f(X_r)dr|\mathcal{F}_s\right]$$

Again by (7), the first term comes out. And because of convergence in the supremum norm we can interchange the expectation and integral. So

$$\begin{aligned}
\mathbb{E}^{X_0}\left[\int_0^t \mathrm{L}f(X_r)dr|\mathcal{F}_s\right] &= \int_0^s \mathrm{L}f(X_r)dr + \int_s^t \mathbb{E}^{X_0}\left[\mathrm{L}f(X_r)|\mathcal{F}_s\right]dr \\
&= \int_0^s \mathrm{L}f(X_r)dr + \int_s^t \mathbb{E}^{X_s}\left[\mathrm{L}f(X_{r-s})\right]dr \\
&= \int_0^s \mathrm{L}f(X_r)dr + \int_s^t \frac{d}{dr}\mathbb{E}^{X_s}\left[f(X_{r-s})\right]dr \\
&= \int_0^s \mathrm{L}f(X_r)dr + \mathbb{E}^{X_s}\left[f(X_{t-s})\right] - \mathbb{E}^{X_s}\left[f(X_0)\right] \\
&= \int_0^s \mathrm{L}f(X_r)dr + \mathbb{E}^{X_s}\left[f(X_{t-s})\right] - f(X_s)
\end{aligned}$$

The second equality is because of the Markov property. then we use lemma 1 [14] and evaluate the boundary terms. Putting it altogether gives

$$\mathbb{E}^{X_0}\left[M_t|\mathcal{F}_s\right] = f(X_s) - f(X_0) - \int_0^s \mathrm{L}f(X_r)dr = M_s$$

so we conclude that M is a martingale. □

Lemma 1.

$$\mathbb{E}^\eta\left[\mathrm{L}f(\omega(t)\right] = \frac{d}{dt}\mathbb{E}^\eta\left[f(\omega(t))\right] = \mathrm{L}\left[\mathbb{E}^\eta\left[f(\omega(t)\right]\right]$$

Proof. Fix a $t \geq 0$ and let $h > 0$. ξ is like ω a generic element of D_Y. Then

$$\mathbb{E}^\eta\left[\frac{\mathbb{E}^{\omega(t)}\left[f(\xi(h))\right] - f(\omega(t))}{h}\right] = \frac{\mathbb{E}^\eta\left[\mathbb{E}^{\omega(t)}\left[f(\xi(h))\right]\right] - \mathbb{E}^\eta\left[f(\omega(t))\right]}{h}$$

$$= \frac{\mathbb{E}^\eta\left[\mathbb{E}^\eta\left[f(\omega(t+h))|\mathcal{F}_t\right]\right] - \mathbb{E}^\eta\left[f(\omega(t))\right]}{h}$$

$$\mathbb{E}^\eta\left[\frac{\mathbb{E}^{\omega(t)}\left[f(\xi(h))\right] - f(\omega(t))}{h}\right] = \frac{\mathbb{E}^\eta\left[f(\omega(t+h))\right] - \mathbb{E}^\eta\left[f(\omega(t))\right]}{h} \tag{2}$$

The second equality uses the Markov property at last we use (9). Let $h \searrow 0$ then the right hand side of (2) is by definition the derivative. And because the expectation is a bounded linear operator, it is continuous as well. So the left hand side converges to the expectation of Lf. For the second equality we start from the right hand side (2) and use again the Markov property but now at time h:

$$\frac{\mathbb{E}^\eta\left[f(\omega(t+h))\right] - \mathbb{E}^\eta\left[f(\omega(t))\right]}{h} = \frac{\mathbb{E}^\eta\left[\mathbb{E}^\eta\left[f(\omega(t+h))|\mathcal{F}_h\right]\right] - \mathbb{E}^\eta\left[f(\omega(t))\right]}{h}$$

$$= \frac{\mathbb{E}^\eta\left[\mathbb{E}^{\omega(h)}\left[f(\xi(t))\right]\right] - \mathbb{E}^\eta\left[f(\omega(t))\right]}{h}$$

Take the limit $h \searrow 0$ and we get the desired result for the second equality. □

7 Applications to model

In this section we apply the results of the preceding sections to our model defined in section 4.2. Finally we will see some results of our efforts to become acquainted with the theoretical framework. We will find an expression for the asymptotic velocity of the SUV:

$$\lim_{t\to\infty} \frac{Z_t}{t}$$

and see that (asymptotically) the position Z_t has a normal distribution. The latter is an example of a central limit theorem (abbreviation: CLT) for additive functionals on a Markov process. Now let us make the last theoretical steps towards this goal.

As we saw earlier Z_t increases or decreases with 8 nm when certain transitions $\eta \mapsto \eta'$ occur. The times at which these transitions occur follow a Poissonian distribution. This reminds us of a Poisson process N_t with rate λ. Because there N_t increases with 1 at Poisson distributed times. It has the following property:

Proposition 1. *The process M on $\mathbb{N}$ with*

$$M_t = N_t - \lambda t$$

is a martingale with respect to $\{\mathcal{F}_t\}_{t\geq 0}$ with $\mathcal{F}_t = \sigma\{N_s : t \geq s \geq 0\}$

Proof. The first property of definition 4 is accounted for by construction and we have the second requirement since $\forall t \geq 0$:

$$\mathbb{E}\left[M_t\right] = \mathbb{E}\left[N_t\right] - \lambda t = \lambda t - \lambda t = 0$$

For checking the third property of a martingale we choose an s, s' such that $t \geq s' \geq s \geq 0$. Then because of (7) we have

$$\mathbb{E}\left[N_t - \lambda t|\mathcal{F}_s\right] = \mathbb{E}\left[N_t - \lambda t - N_s + \lambda s|\mathcal{F}_s\right] + N_s - \lambda s$$

$$= \mathbb{E}\left[N_t - N_s|\mathcal{F}_s\right] + \lambda(s-t) + N_s - \lambda s$$

$$= \lim_{s' \searrow s} \mathbb{E}\left[N_t - N_{s'} | \mathcal{F}_s\right] + \lambda(s-t) + N_s - \lambda s$$
$$= \lim_{s' \searrow s} \lambda(t-s') + \lambda(s-t) + N_s - \lambda s$$
$$= N_s - \lambda s$$

□

Another way to prove Prop. 1 is to recognize the Poisson process as a Markov process on $\mathbb{N}$ with generator $\mathrm{L}g(n) = \lambda\left[g(n+1) - g(n)\right]$. If we apply Th. 2 with $f(n) := n$, then we get the same result.

This result is important for us since

$$M_t = Z_t - \int_0^t \psi(\omega(t))ds \tag{3}$$

is also a martingale analogous to $N_t - \lambda t$. We will specify ψ in a moment. In both cases the second term is an integral over the rates. Such an integral over time of a functional on S is called an additive functional on a stochastic process. M_t represents the fluctuation of the process away from its average increment over time. Intuitively this varies around zero and that is exactly what a (mean zero) martingale does. ψ represents the average rate at which the SUV moves, so we have defined it as follows for ζ in S:

$$\psi(\zeta) = \psi^+(\zeta) - \psi^-(\zeta) = \sum_{\eta \mapsto \eta' \in R^+} q(\eta, \eta')\mathbf{1}_{\{\zeta=\eta\}} - \sum_{\widetilde{\eta} \mapsto \widetilde{\eta}' \in R^-} q(\widetilde{\eta}, \widetilde{\eta}')\mathbf{1}_{\{\zeta=\widetilde{\eta}\}} \tag{4}$$

We want to know an expression for the asymptotic velocity. If we take the limit $t \to \infty$ of both sides of (3) the LHS will converge in distribution to zero since it is a martingale. So we have in distribution:

$$\lim_{t\to\infty} \frac{Z_t}{t} = \lim_{t\to\infty} \frac{1}{t} \int_0^t \psi(\omega(t))ds$$

Using Birkhoff's ergodic theorem [4] the integral term converges almost surely to the integral of ψ over the state space with respect to the invariant measure μ:

$$\lim_{t\to\infty} \frac{1}{t} \int_0^t \psi(\omega(t))ds = \int \psi(\eta)\mu(d\eta)$$

So this is almost surely our expression for the velocity:

$$\lim_{t\to\infty} \frac{Z_t}{t} = \int \psi(\eta)\mu(d\eta) = \sum_{\eta \in S} \mu(\eta)\,\psi(\eta) := \mathrm{v} \tag{5}$$

v can explicitly be calculated as we know ψ and in chapter 6 we noted that finding μ comes down to solving a (finite) system of linear equations.

At the same time this imposes a practical problem, because when the size of the vesicle becomes in the order if $1\mu m$ (which is experimentally reasonable), the number of different sites will be a little more than 100. But the number

of possible configurations η will be enormously bigger, at least 2000. In principle solving a linear system of 2000 equations can be done then the entries are numeric,but the biggest problem is to define the L matrix in a computer. Inserting every entry by hand takes too much time and there is no way to automate the assignment of configurations and rates. So eventually we did not obtain an explicit formula for the velocity of our model from section 2.2 this way. Nevertheless it did work for a much simpler model. See appendix B for the explicit calculations with this simple model that consists of a MT lattice of only two sites.

We have dealt with the mean velocity. Now it is time to shift our attention to the asymptotic distribution of Z_t. We will proof that as $t \to \infty$ in distribution

$$\frac{Z_t - \mathrm{v}t}{\sqrt{t}} \longrightarrow \mathrm{N}(0, \sigma^2)$$

From (3) it follows that for all $t \geq 0$:

$$Z_t - \mathrm{v}t = \int_0^t \psi(\omega(t)) - \mathrm{v}ds + M_t \tag{6}$$

We recognize the first term of the RHS of (6) as a additive functional on S. Now we want to apply theorem 2 to replace that term by a martingale. But we can not yet insert theorem 2 immediately because we have an integral over $\psi - \mathrm{v}$ instead of $\mathrm{L}f$. We proof now that $\psi - \mathrm{v}$ lies in the image of L. Notice from the construction of v that for the invariant measure μ: $\int [\psi - \mathrm{v}] d\mu = 0$.

Proposition 2. *Let X be a finite Markov chain with generator* L*, then the following equality holds:*

$$\mathrm{Im}\,(\mathrm{L}) = \left\{ \psi \in C_b(S) : \int \psi d\mu = 0 \right\}$$

Proof. From linear algebra we know that

$$\mathrm{Im}\,(\mathrm{L}) = \mathrm{Ker}\left(\mathrm{L}^{\mathrm{T}}\right)^{\perp}$$

Furthermore

$$\begin{aligned} \mathrm{Ker}\left(\mathrm{L}^{T}\right) &= \left\{ \mu^T \in C_b(S) : \mathrm{L}^T \mu^T = 0 \right\} \\ &= \{ \mu' : \mu' \mathrm{L} = 0 \} \end{aligned}$$

But we know that this is a one dimensional subspace, since we have found the unique measure μ such that $\mu \mathrm{L} = 0$. So

$$\begin{aligned} \mathrm{Im}\,(\mathrm{L}) &= \{\mu\}^{\perp} \\ &= \{ \psi \in C_b(S) : \langle \psi, \mu \rangle = 0 \} \\ &= \left\{ \psi \in C_b(S) : \int \psi d\mu = 0 \right\} \end{aligned}$$

□

This proposition relies heavily on the fact that we have a finite state space. The general case is much more subtle. We refer to the next chapter for details about ψ lying in the image of L in the infinite dimensional case. Putting (1) and (6) together we obtain:

$$Z_t - \mathrm{v}t = \widetilde{M}_t + \phi(X_0) - \phi(X_t) + M_t$$

with $-\mathrm{L}\phi = \psi - \mathrm{v}$ and $\widetilde{M}$ the martingale from theorem 2 and M the martingale from (3). The sum of two martingales is again a martingale and since $\mathbb{E}[M_0] = \mathbb{E}[\widetilde{M}_0] = 0$, we conclude with the aid of theorem 4 and the fact that ϕ is bounded (so the ϕ terms vanish in the limit): if $t \to \infty$ then we have the following convergence in distribution

$$\frac{Z_t - \mathrm{v}t}{\sqrt{t}} \longrightarrow \mathrm{N}(0, \sigma^2)$$

Stationarity and ergodicity is met since we have an irreducible finite Markov chain. This is the central limit theorem for Z_t, the additive functional on our Markov process X. It remains unclear if we can say anything more about the value of σ^2.

8 CLT for additive functionals on a stationary ergodic Markov process

In the previous section, we proved a CLT for additive functionals on a Markov process. Z_t, the position of the SUV converges to a normal distribution with an unknown σ^2. The proof relied heavily on the fact that in our model the state space is finite. In this chapter we focus on the general case of a Markov process with a possibly uncountable state space. Then situation becomes much more intricate. First of all L is not necessarily a bounded operator anymore, so the domain is not equal to $C_b(Y)$ but only the set of bounded functions f for which the limit

$$\mathrm{L}f(\eta) = \lim_{t \to 0} \frac{\mathbb{E}^\eta[f(\omega(t)] - f(\eta)}{t}$$

exists for all $\eta \in Y$.

Secondly and this even more important for our CLT, the condition that $\int \psi d\mu = 0$ is not sufficient anymore for the existence of a ϕ: $\mathrm{L}\phi = \psi$, in contrast with Prop 2. Kipnis and Varadhan prove in [6] the CLT for additive functionals under virtually no assumptions other than the necessary ones.

Theorem 3. *Let X be a Markov process with generator* L*, reversible with respect to a probability measure μ, and let us suppose that the reversible stationary process P with μ as invariant measure is ergodic. Let ψ be a function on the state space that lies in $L_2(\mu)$, satisfying $\int \psi d\mu = 0$ and $\psi \in \mathrm{D}((-\mathrm{L})^{-\frac{1}{2}})$. finally let*

$$\widetilde{Z}_t = \int_0^t \psi(X_s) ds$$

then there exists a square integrable martingale M with respect to filtration $\{\mathcal{F}_t\}_{t\geq 0}$ such that M has stationary increments and

$$\lim_{t\to\infty} \frac{1}{\sqrt{t}} \sup_{t\geq s\geq 0} |\widetilde{Z}_s - M_s| = 0$$

in probability with respect to P where $\widetilde{Z}_0 = M_0 = 0$.

Here we give an overview of the theorem and its proof rather than a detailed account. Kipnis and Varadhan proof this theorem in [6] with the additional constraint that the process is reversible. This means that the generator L is a symmetric operator [8] in $L_2(\mu)$:

$$\forall f, g \in L_2(\mu) : \langle \mathrm{L}f, g\rangle = \langle f, \mathrm{L}g\rangle$$

In our case the process does not satisfy reversibility so then an uncountable state space would become even more difficult.

We see that the Markov process needs to be stationary and ergodic. This guarantees in fact the conditions of stationary and ergodic increments in theorem 4. This requirement is met in our model. Notice that if we would ignorantly (and erroneously because of the reversibility) apply this theorem to our model, $\widetilde{Z}_t$ would not be the position Z_t but only the integral term of the RHS of (6) as the notation also suggests. This is also one of the main reasons why we have not found an explicit expression for the variance of the normal distribution, because of the possible covariance of the two martingale terms in (6).

The special necessary requirement that is different from the finite dimensional case, for the existence of ϕ is that it needs to be in the domain of $(-\mathrm{L})^{-\frac{1}{2}}$. If that is satisfied we can apply theorem 4 once again and prove the CLT.

The outline of the proof is as follows. Since X is a reversible Markov process, the generator L is self-adjoint on $L_2(\mu)$. This implies that L admits a spectral decomposition such that $\forall \psi \in L_2(\mu)$:

$$\langle \psi, \mathrm{L}\psi\rangle = \int_{\sigma(\mathrm{L})} \lambda \, \mu_\psi(d\lambda)$$

where $\sigma(\mathrm{L})$ is the spectrum of L and $\mu_\psi(d\lambda)$ the spectral measure of ψ. If we want σ^2 to be finite, this comes down to checking that $\int \frac{1}{\lambda}\mu_\psi(d\lambda) < \infty$ Which is in fact equivalent to saying that ψ needs to lie in $\mathrm{Im}((-\mathrm{L})^{\frac{1}{2}})$, which can be expressed as $\psi \in D((-\mathrm{L})^{-\frac{1}{2}})$. Digging deeper into the proof of this theorem would go beyond the purposes of this thesis. But it is nice to end with this, as it makes clear that for me there is still a lot to learn.

A Matlab code of simulations

See next page for the code.

B Simplified model of two bindingsites

In this appendix we discuss a simplified model with one lattice containing of 2 sites. The reason that we have developed this, is that the number of configurations for our model from section 4.2 is always too big for symbolic calculations as we discussed in section 7. The left site (denotes minus end) can either be empty or dynein can bind to it. Likewise for the right (plus end) but there a kinesin can bind. In this way we have four possible configurations (see figure 14), which is manageable.

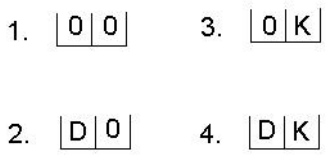

Figure 14: All possible configurations. The enumeration comes in handy when we define our generator matrix L. Note that configuration 1 represents the SUV not being bound to the MT.

We proceed with all possible transitions. Not every transition rate can be expressed in the single motor parameters from section 4.2 since we use here a sort of mean field approximation. We denote the rate with which a dynein binds with c and the binding rate for kinesin with j the other parameters are the same. For clarity we have named the parameters from section 4.2 differently. In this way we do not have to deal with all the sub- and superscripts. $l = k_f^K, e = k_f^D, f = k_u^D, m = k_u^K$. Note that we distinguish now between the unbinding rate of kinesin versus dynein. Later on we can always insert the known value from section 4.2. A last parameter is the back stepping rate h of dynein. See figure 15 for the possible transitions.

This results in the following generator matrix L.

$$\mathrm{L} = \begin{pmatrix} -c-j & c & j & 0 \\ f & -f-j & 0 & j \\ m & 0 & -c-m & c \\ 0 & m+\frac{em}{e+m} & f+\frac{fl}{f+l} & -f-\frac{fl}{f+l}-m-\frac{em}{e+m} \end{pmatrix}$$

With mathematica we have solved the equation $x\mathrm{L} = 0$. This resulted in.

$$x = \begin{pmatrix} -\frac{f+\frac{fl}{f+l}}{j} + \frac{(-c-m)\left(-(-f-j)j\left(-f-\frac{fl}{f+l}-m-\frac{em}{e+m}\right)+j\left(-c\left(f+\frac{fl}{f+l}\right)+j\left(m+\frac{em}{e+m}\right)\right)\right)}{j(-c(-f-j)j-cj(-c-m))} \\ \frac{+2cefm+ef^2m+2efjm+2celm+2eflm+2ejlm+cfm^2+2efm^2+f^2m^2+fjm^2+clm^2+2elm^2+2flm^2+jlm^2+fm^3+lm^3}{j(f+l)(e+m)(c+f+j+m)} \\ -\frac{-(-f-j)j\left(-f-\frac{fl}{f+l}-m-\frac{em}{e+m}\right)+j\left(-c\left(f+\frac{fl}{f+l}\right)+j\left(m+\frac{em}{e+m}\right)\right)}{-c(-f-j)j-cj(-c-m)} \\ 1 \end{pmatrix}$$

We want a probability measure μ so we normalize x to obtain μ.

$$\mu = \frac{x}{\sum_{\eta\in\Omega} x\left(\eta\right)}$$

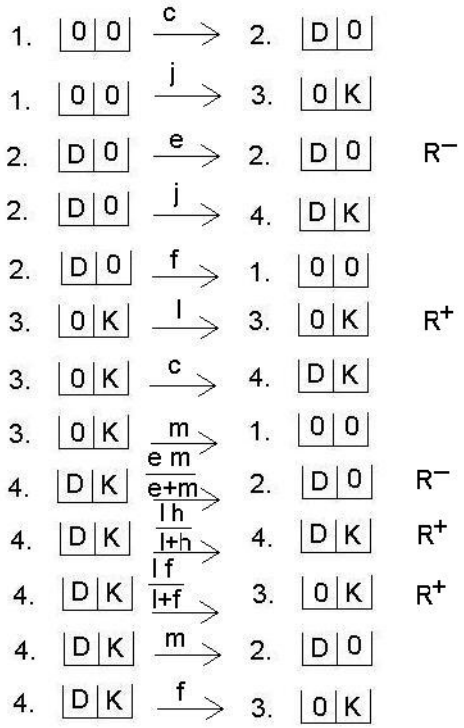

Figure 15: All possible transition. The rates of the transitions are situated above the arrows. Some transitions involve two motors, that is why there are three transition rates that are not just a single motor parameter. The transitions that induce the SUV to step towards the plus end have a R^+ ont the right, similarly for movement of the SUV to the minus end we have R^-

We proceed with the velocity. We use equation (4) to get:

$$\psi = \begin{pmatrix} 0 \\ -e \\ l \\ \frac{lf}{l+f} + \frac{lh}{l+h} - \frac{em}{e+m} \end{pmatrix}$$

Now we have a expression for equation (5), the speed v. Unfortunately since we do not know the parameters c and j , we can not insert numerical values. c and j are related to the single motor binding rates and the invariant measure μ.

C Martingales and conditional expectations

This section presents some definitions and properties of martingales. For this we need a notion of conditional expectation. For a more detailed account, including proofs, we refer to [12].

Definition 3. *let $(\Omega, \mathcal{A}, \mathbf{P})$ be a probability space and X a random variable on it with $\mathbb{E}[|X|] < \infty$. Furthermore $\mathcal{F}$ denotes a σ-algebra that is contained in $\mathcal{A}$. Then there exists a random variable Y such that:*

1. *Y is $\mathcal{F}$ measurable.*
2. *$\mathbb{E}[|Y|] < \infty$*
3. *for every set $F \in \mathcal{F}$ we have $\int_F X d\mathbf{P} = \int_F Y d\mathbf{P}$*

We denote Y as $\mathbb{E}[X|\mathcal{F}]$. The existence is guaranteed by the Radon-Nikodym theorem, and Y is $\mathbf{P}$ almost surely unique. We present now some properties of the conditional expectation that we used in this thesis. Let X, X_1 and X_2 be random variables with the necessary properties and $\mathcal{H}$ a sub σ-algebra of $\mathcal{F}$, then

1. if X is $\mathcal{F}$ measurable then almost surely
$$\mathbb{E}[X|\mathcal{F}] = X \tag{7}$$
2. (linearity)
$$\mathbb{E}[X_1 + X_2|\mathcal{F}] = \mathbb{E}[X_1|\mathcal{F}] + \mathbb{E}[X_2|\mathcal{F}] \tag{8}$$
3. almost surely
$$\mathbb{E}[\mathbb{E}[X|\mathcal{F}]|\mathcal{H}] = \mathbb{E}[X|\mathcal{H}] \tag{9}$$

We proceed with the definition of a martingale as we have considered all the preliminary definitions.

Definition 4. *A process M is called a martingale with respect to $\{\mathcal{F}_t\}_{t\geq 0}$ if*

1. *$\forall t \geq 0:$ M_t is $\mathcal{F}_t$-measurable.*
2. *$\mathbb{E}[|M_t|] < \infty$*
3. *$\mathbb{E}[M_t|\mathcal{F}_s] = M_s$ for $t \geq s \geq 0$ almost surely*

For the sake of simplicity we use the discrete time martingale in the remainder of this section, but everything is also valid in the continuous case. Now we notice that we can write every martingale as a sum of increments:

$$M_n = \sum_{i=1}^{n} \Delta_i$$

with Δ_i defined as

$$\Delta_i = \mathbb{E}\left[M_n|\mathcal{F}_i\right] - \mathbb{E}\left[M_n|\mathcal{F}_{i-1}\right]$$

When these increments are all independent and identical distributed we obtain the classical central limit theorem that we all know from secondary school. But the requirements can be loosened without the loss of convergence. Here we present the central limit theorem for martingales that we used in section 7 [8]. Note that the theorem also holds for continuous time martingales.

Theorem 4. *Let $M = \{M_j\}_{j\geq 0}$, with $M_0 = 0$, be a martingale with respect to filtration $\{\mathcal{F}_j\}_{j\geq 0}$ and assume that the increments are stationary and ergodic. Then the distribution function of $\frac{M_n}{\sqrt{n}}$ converges to a normal distribution $\mathrm{N}\left(0,\sigma^2\right)$ as $n \to \infty$, with $\sigma^2 = \mathbb{E}(M_1^2)$.*

We see that only stationary and ergodic increments are required. The first says that $\forall k, i_1..i_k, \tau \in \mathbb{N}$ the following equality of the joint distribution functions holds:

$$\mathbf{F}_{\Delta_{i_1}..\Delta_{i_k}}\left(x_{i_1},...x_{i_k}\right) = \mathbf{F}_{\Delta_{i_1+\tau}..\Delta_{i_k+\tau}}\left(x_{i_1},...x_{i_k}\right)$$

The joint distribution function is invariant under time shifts. And ergodicity means in this case that the increments satisfy Birkhoff's ergodic theorem [4].

References

[1] B. Alberts et al. (2002) *Molecular biology of the Cell, 4^{th}ed.*, Garland

[2] O. Campàs et al. (2006), *Collective dynamics of interacting molecular motors*, Phys. Rev. Lett. 97, 038101

[3] O. Campàs et al. (2008), *Coordination of kinesin motors pulling on fluid membranes*, Biophys. J. 94, 5009-5017

[4] V. Genon-Catalot et al.(2000), *Stochastic volatility models as hidden Markov models and statistical applications*, Bernoulli 6(6), 1051-1079

[5] S.P. Gross (2004), *Hither and yon: a review of bi-directional microtubule-based transport* Phys. Biol. 1, R1-R11

[6] C. Kipnis, S.R.S. Varadhan (1986), *Central limit theorem for additive functionals of reversible Markov processes and applications to simple exclusions*, Commun. Math. Phys. 104, 1-19

[7] A. Kunwar et al. (2008), *Stepping, strain gating, and an unexpected force-velocity curve for multilple-motor based transport*, Curr. Biol. 18, 1173-1183

[8] C. Landim, T. Komorowski, S. Olla, *Fluctuations in Markov processes*, book in progress, http://w3.impa.br/ landim/notas.html

[9] A. De Masi, P.A. Ferrari (1989), *An invariance principle for reversible Markov processes. Applications to random motions in random environments*, J. Stat. Phys. 55(3-4),787–855

[10] M. Müller et al. (2008), *Motility states of molecular motors engaged in a stochastic tug-of-war*, J. Stat. Phys. 133, 1059-1081

[11] S.L. Reck-Peterson et al. (2004), *Molecular dissection of the roles of nucleotide binding and hydrolysis in dynein's AAA domains in Saccharomyces cerevisiae*, Proc. Natl. Acad. Sci. USA 101, 1491–1495.

[12] L.C.G. Rogers, D. Williams (1979), *Diffusions, Markov Processes, and Martingales, Vol. I*, Wiley

[13] L. Saunders, J. Perrin and D. Gammack (1962), *Ultrasonic irradiation of some phospholipid sols.*, J. Pharm. Pharmacol. 14,567–572.

[14] T. Seppäläinen, *Translation Invariant Exclusion Processes*, book in progress, http://www.math.wisc.edu/ seppalai/excl-book/etusivu.html

[15] M.P. Sheetz (1999), *Motor and cargo interactions*, Eur. J. Biochem. 262, 19-25

[16] S. Verbrugge et al. (2007), *Kinesin Moving through the Spotlight: Single-Motor Fluorescence Microscopy with Submillisecond Time Resolution*, Biophys. J. 92, 2536-2545

[17] Z. Wang, M.P. Sheetz (1999), *One-dimensional diffusion on microtubules of particles coated with cytoplasmic dynein and immunoglobulins*, Cell Struct. Funct. 24, 373–383

[18] E.C. Young et al. (1995), *Subunit interactions in dimeric kinesin heavy chain derivatives that lack the Kinesin rod*, J. Biol. Chem. 270, 3926-3931